Materials Science & Engineering A 654 (2016) 256–263

Contents lists available at ScienceDirect

Materials Science & Engineering A

journal homepage: www.elsevier.com/locate/msea

Anomalies in the deformation mechanism and kinetics of coarse-grained high entropy alloy

Mageshwari Komarasamy [a], Nilesh Kumar [a], Rajiv S. Mishra [a,*], Peter K. Liaw [b]

[a] Center for Friction Stir Processing, Department of Materials Science and Engineering, University of North Texas, Denton, TX 76203, USA
[b] Department of Materials Science and Engineering, The University of Tennessee, Knoxville, TN 37996, USA

ARTICLE INFO

Article history:
Received 6 November 2015
Received in revised form
17 December 2015
Accepted 18 December 2015
Available online 19 December 2015

Keywords:
High entropy alloy
Mechanical characterization
Transient tensile tests
Dislocations
Plasticity

ABSTRACT

Starting from the thermodynamics to thermal and mechanical properties, high entropy alloys (HEAs) always deviate from the behavior of conventional materials and stamp its uniqueness among the alloy systems. In this study, tensile deformation mechanisms of HEA was investigated. A simple system, an $Al_{0.1}$CoCrFeNi HEA, with a single crystal structure (face-centered cubic, FCC), coarser grains (CG), and low dislocation density was chosen to exclusively study the effect of intrinsic lattice on the HEA deformation mechanisms and kinetics. Monotonic tests were done at the strain rate of 10^{-3} s^{-1}, and all the transient tests were started at the initial strain rate of 10^{-3} s^{-1}. Strain-jump tests were carried out at strain rates of 10^{-5} s^{-1} and 10^{-3} s^{-1}. Repeated stress relaxation tests were performed along the stress–strain curve to calculate the physical activation volume. Surprisingly, a large rate sensitivity of the flow stress and low activation volume of dislocations were observed, which are unparalleled, as compared to conventional CG FCC metals and alloys. The observed trend has been explained in terms of the lattice distortion and dislocation-energy framework. As opposed to the constant dislocation line energy and Peierls potential energy (amplitude, ΔE) in conventional metals and alloys, both the line energy and Peierls potential undergo continuous variations in the case of HEAs. These energy fluctuations have greatly affected the dislocation mobility and can be distinctly noted from the activation volume of dislocations.

1. Introduction

High entropy alloys (HEAs), by definition, constitute a minimum of five elements in equimolar or non-equimolar quantities (between 5% and 35%). The conception to form HEAs was mainly based on the Boltzmann hypothesis where the contribution of the configurational entropy of mixing (ΔS_{mix}) to the free energy increases with the number of elements and contributes in the formation of random solid solution. Yeh et al. [1] and Cantor et al. [2] were the first ones to test the hypothesis and were successful in synthesizing the high entropy alloy solid solutions of various compositions having simple face-centered cubic (FCC) or body-centered cubic (BCC) crystal structure. Though it crystallizes in simple crystal structures, FCC [1–5], BCC [4–6] or hexagonal close-packed (HCP) [7,8], severe lattice distortion is inevitable because the high entropy alloy generally constitutes elements of varying sizes and cohesive energies. The lattice distortion will have its consequences on atomic diffusion, creep resistance, and on the mechanical properties. Tsai et al. [9] have incorporated lattice distortional effects in their study and concluded that the sluggish diffusion in HEA is due to low potential energy (LPE) valleys which served as atomic traps. A recent study by Mishra et al. [10] highlighted the importance and effect of lattice distortion/strain on the deformation mechanisms, particularly the energetics and kinetics of slip and twinning in HEA. Kumar et al. [11] have calculated the lattice strain for various HEAs and found out that the lattice strain is significantly higher in Al containing HEAs as compared to the CoCrFeMnNi HEA system. Although the correlation between the presence of Al and the increase in the hardness is quite known, the underlying dislocation mechanisms responsible for such observation was not specifically discussed before [4,12].

Though there are numerous efforts concerning the mechanical properties of various HEAs [13–16], there are only a handful of studies regarding the fundamental understanding of the plastic deformation mechanisms in HEAs. Major observations from limited published literatures are summarized in what follows here. Otto et al. [17] studied the effect of temperature and grain size on the deformation of the CoCrFeMnNi HEA. They observed severe temperature dependence of mechanical properties. Moreover, extensive twinning was observed at 77 K as opposed to dislocation-dominated deformation at room temperature. In a study on $Al_{0.1}$CoCrFeNi HEA, Komarasamy et al. [18] have studied the work

* Corresponding author.
E-mail address: Rajiv.Mishra@unt.edu (R.S. Mishra).

http://dx.doi.org/10.1016/j.msea.2015.12.063
0921-5093/

hardening behavior of both coarse-grained (CG) and fine-grained (FG) high-entropy alloy. In contrast to the CoCrFeMnNi alloy, they observed extensive deformation twinning in the CG $Al_{0.1}$CoCrFeNi HEA at room temperature and at quasi-static strain rate conditions. This distinctive observation was later justified based on a lattice strain framework [10]. The CoCrFeMnNi HEA also exhibited exceptional fracture toughness at cryogenic temperatures (77 K) and the high values were attributed to the nano-scale deformation twinning [19]. Hemphill et al. [20] have reported high resistance to fatigue failure and a very high fatigue endurance limit in the $Al_{0.5}$CoCrCuFeNi HEA. In another study, Wu et al. [21] explained the severe temperature dependence of yield strength, basically the lattice friction stress, in terms of the Peierls potential barrier height. The barrier strength in the CoCrFeMnNi HEA was found to be stronger than pure FCC metals, but weaker than BCC metals. Besides the strong temperature dependence of yield strength, large lattice friction stress values were also reported in $Al_{0.1}$CoCrFeNi [22] and CoCrFeMnNi [17] HEAs. Though the underlying concepts were not explicitly discussed in most of the studies, the experimental evidences so far gives a distinctive identity to the nature and motion of dislocations in FCC HEA as compared to the conventional FCC metals and alloys. As discussed earlier, exceptional mechanical properties have been reported for various HEAs, but an in-depth understanding of the underlying deformation mechanism is still lacking.

In the current study, we have investigated the deformation mechanism of the CG $Al_{0.1}$CoCrFeNi HEA. Our principal objective was to investigate the thermally activated dislocation mechanisms in HEAs. To achieve the proposed aim, transient tests, both strain rate jump tests and stress relaxation tests, were conducted at room temperature. The tests yielded the strain-rate sensitivity of the flow stress and physical activation volume of dislocations. Since, there are only two studies available on the strain rate sensitivity or the activation volume of the FCC HEAs, the results for conventional FCC metals and alloys were mostly taken as the reference. The physical activation volume or dislocation sweep area holds the key to understanding the dislocation motion during a thermal activation event. The effect of either the microstructural features or the lattice itself on such dislocation processes can be readily recognized from the activation volume values. As a result of this endeavor, we present both the strain rate sensitivity and activation volume values of HEAs, and for the very first time, a detailed discussion on the theoretical lattice-dislocation energy framework to explain the observed peculiar trends.

2. Experimental procedure

The $Al_{0.1}$CoCrFeNi HEA was prepared by vacuum induction melting followed by hot isostatic pressing (HIP) at 103.4 MPa and 1478 K for 4 h. The following initial characterization was conducted: X-ray diffraction (XRD), orientation imaging microscopy (OIM), scanning electron microscopy (SEM) in back-scattered electron (BSE) mode, and transmission electron microscopy (TEM). The XRD analysis was performed in Rigaku III Ultima X-ray diffractometer with Cu K_α radiation of wavelength 0.1542 nm. OIM was done in FEI Nova NanoSEM 230 interfaced with TSL™ electron back scattered diffraction (EBSD) system.

The sample for the EBSD analysis was polished down to 1 μm surface finish using colloidal diamond polishing solution and then to 0.02 μm surface finish using colloidal silica suspension. The samples for tensile testing were polished down to ~1 μm surface finish using diamond polishing solution. Both the monotonic and transient tensile tests were performed on a custom-built computer controlled tensile testing machine operated in a displacement controlled mode. Dog-bone shaped mini-tensile specimens of gage size, length of 5 mm, width of ~1.23 mm, and thickness of ~1.10 mm were used. The monotonic tests were carried at an initial strain rate of $1\times10^{-3}\,s^{-1}$ and at room temperature. The cross-head velocity (gage length × initial strain rate) was maintained constant throughout the test. All the strain rate jump tests were started with the monotonic strain rate of $1\times10^{-3}\,s^{-1}$ and rate jumps were made between $1\times10^{-3}\,s^{-1}$ and $1\times10^{-5}\,s^{-1}$ strain rates. Strain rate jumps were made at various strains along the stress–strain curve and five samples were tested for statistical validation. Even the repeated stress-relaxation tests were started with the strain rate of $1\times10^{-3}\,s^{-1}$ and then the cross head movement was stopped while the data acquisition was still going on to record the stress drop as a function of time. The stress relaxations were carried out for 100 s and then, the specimen was loaded back to the same stress as the starting point of the first relaxation cycle. The relaxation cycles were repeated for 5-6 times and the relaxation cycle sets were repeated at various strains.

3. Results

3.1. Initial microstructural characterization

The initial microstructural characterization was carried out using OIM, XRD, and TEM analyses, and the results are shown in Fig. 1(a) and (b). From the OIM micrograph, it is evident that the grains are very coarse-on the order of millimeter in size. The XRD peaks in Fig. 1(b) correspond to the FCC crystal structure and the absence of other peaks indicates that the material contains only FCC phase. The shoulder peaks can be certainly attributed to another FCC phase with a slight variation in the lattice parameter. The lattice parameter calculated based on the major peaks is 0.359 nm. The SAD pattern, inset in Fig. 1(b) (the beam direction is [011]), clearly shows the absence of other spots, which is indicative of the absence of fine precipitates or second phases in the material. The BSE SEM analysis clearly showed the absence of coarse second phase particles (not shown here).

3.2. Tensile test results

Both the engineering stress-engineering strain and true stress-true strain curves of all the four samples tested are shown in Fig. 2 (a) and (b), respectively. The average value of the YS, UTS, UE, and TE are 160 ± 7 MPa, 389 ± 42 MPa, 44 ± 15, and 53 ± 16, respectively. The lower yield strength values can be justified based on the mm sized grains, absence of precipitates, low dislocation density, and the lower Al content. Though the material has shown low YS, it has work hardened quite extensively to reach high strength levels. The material exhibited very large elongation in all the samples tested, in both uniform and non-uniform elongation parts.

3.3. Transient tests

Section 3.2 does not provide insight to the underlying mechanisms and kinetics of the deformation. Therefore, transient tests were utilized to study the fundamental aspects of deformation kinetics in HEAs. The results of both the strain rate jump tests and the repeated stress relaxation tests are discussed in Section 3.3.

3.3.1. Strain-rate-jump tests

3.3.1.1. Strain rate sensitivity. Strain rate jump experiments were performed at finite strain intervals along the uniform part of the stress–strain curve to study the rate sensitivity of the flow stress. Five samples were used for rate jump tests and Fig. 3(a) shows one such sample with series of rate jumps. In the calculation of strain

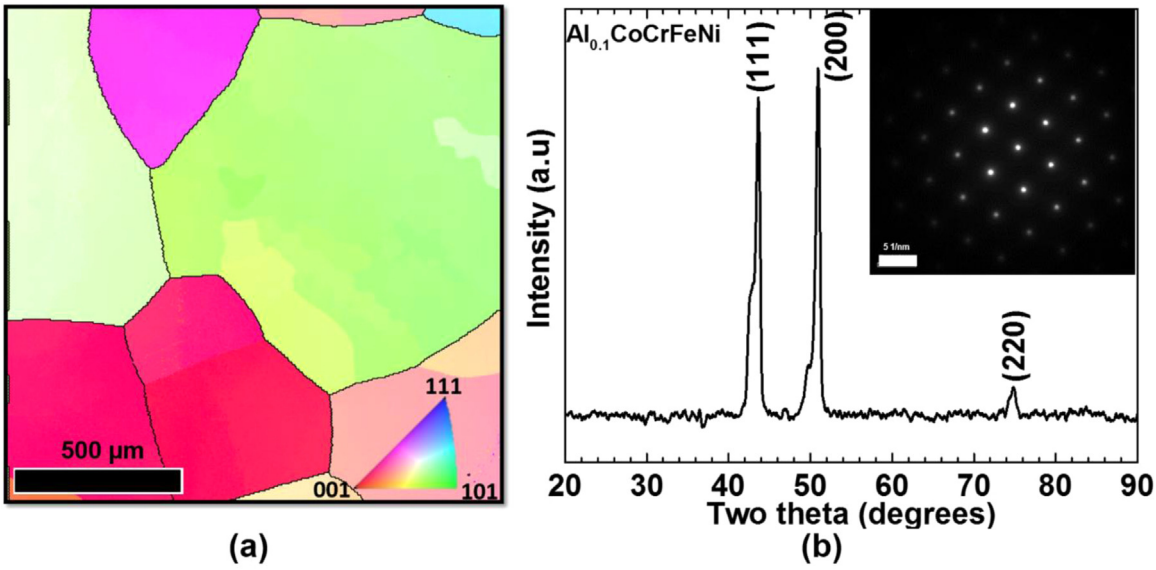

Fig. 1. Initial microstructural characterization of the CG material showing (a) an OIM image [22] and (b) XRD pattern with TEM SAD pattern as inset.

rate sensitivity of the flow stress, only up jumps (from 10^{-5} s^{-1} to 10^{-3} s^{-1} strain rate) were considered. It can be observed from the rate jumps that the flow stress increases with the strain rate, which is known as the positive strain-rate sensitivity of the flow stress. The results of all the tests are compiled and shown in Fig. 3 (b) as a function of plastic strain. The rate sensitivity (m) of the flow stress was calculated based on the following equation [23]

$$m = \frac{\Delta \ln \sigma}{(\Delta \ln \dot{\varepsilon})_{T,\varepsilon}} = \frac{\ln(\frac{\sigma_2}{\sigma_1})}{(\ln \frac{\dot{\varepsilon}_2}{\dot{\varepsilon}_1})_{T,\varepsilon}} \quad (1)$$

where σ is the flow stress, $\dot{\varepsilon}$ the strain rate, and ε the plastic strain. The graph contains m values from five samples tested at various strain levels. Higher rate sensitivity has been observed at the low strain levels (low flow stress, σ) and decreased with the increase in strain (high flow stress, σ). At the low strain levels (below 0.05), m values in the range of 0.02–0.017 were observed, which is 2–3 times higher than a typical FCC CG material's strain rate sensitivity. At larger strain the m value dropped to ~0.007. The observed rate sensitivities of the CG HEA are not of a typical FCC CG materials' response and will be subjected to detailed scrutiny in Section 4.

3.3.1.2. Apparent activation volume. Based on the strain rate jump test results, the apparent activation volume was calculated using the following equation [23]

$$V_a = MkT(\Delta \ln \dot{\varepsilon} / \Delta \sigma) \quad (2)$$

where M is the Taylor factor (3.06), k is the Boltzmann constant, T is the absolute temperature in K, and $\Delta\sigma$ is the stress jump for a given rate jump. The results of the calculation are shown in Fig. 4. The values of the apparent activation volume ranged from 288 b^3 at small strains to 197 b^3 at large strains, where b is the Burgers vector (b=0.2539 nm, from the XRD analysis). The apparent activation volume is extremely small and unusual for a material with such large grains and no other evident microstructural barriers.

The activation volume calculated from the strain rate jump experiments is not the true activation volume of dislocations. According to the Orowan relationship, $\dot{\gamma} = b\rho_m \vartheta$, the strain-rate change is accommodated by the change in both the density (ρ_m) and velocity of mobile dislocations (ϑ). In order to obtain a true activation volume, the contribution of the mobile dislocation velocity has to be separated out from the density change. One way to obtain the dislocation mobility is to perform repeated stress relaxation tests.

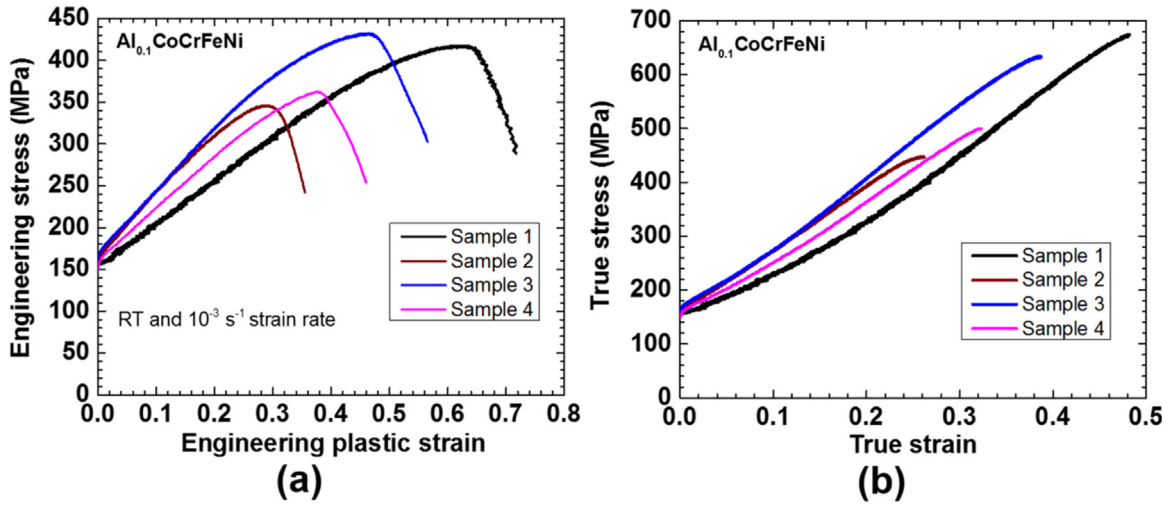

Fig. 2. (a) Engineering stress-engineering strain and (b) true stress-true strain curves of the samples tested in the as-HIPed condition.

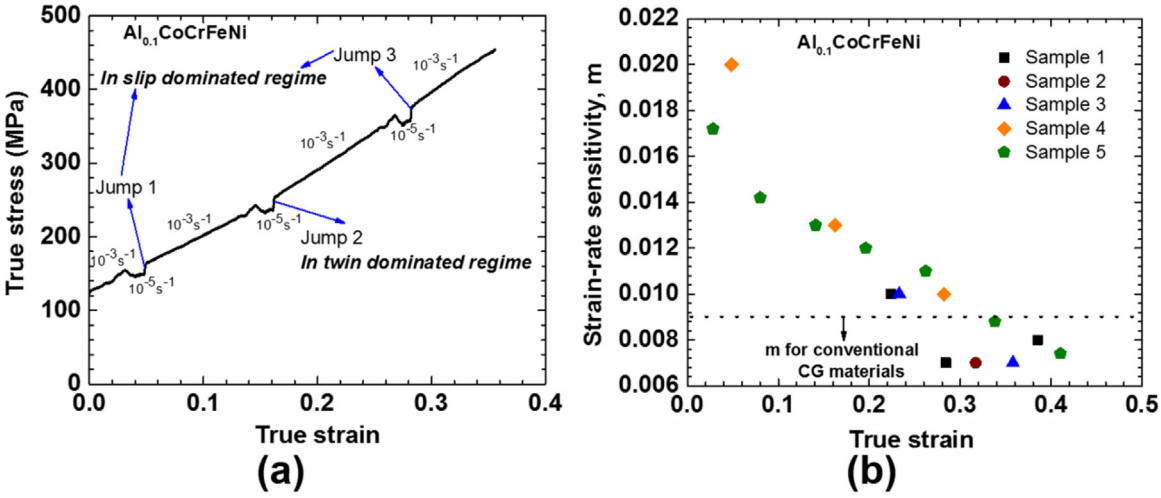

Fig. 3. (a) Strain-rate jump tests along the stress–strain curve at various strain and (b) strain-rate sensitivity as a function of plastic strain gathered from five samples.

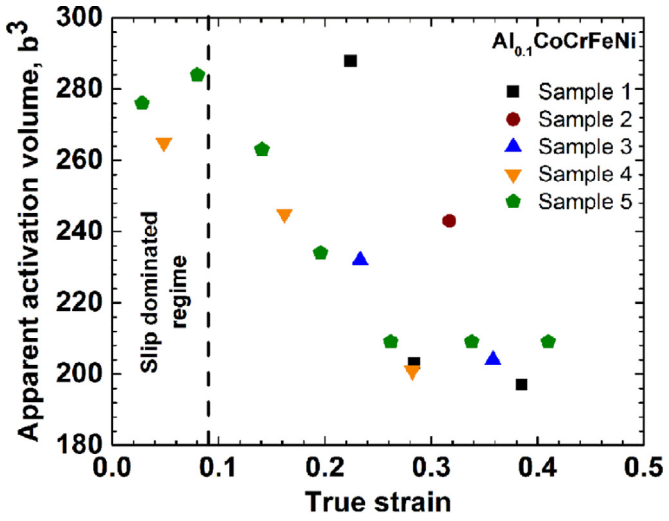

Fig. 4. Apparent activation volume as function of plastic strain calculated from strain rate sensitivity results.

3.3.2. *Repeated stress relaxation tests*

Repeated stress relaxation experiments were carried out at various flow stress levels, to understand the variation in physical activation volume as a function of plastic strain. Fig. 5(a) shows six set of repeated relaxation tests along the true stress–strain curve. From the repeated stress relaxation tests, both the apparent and physical activation volumes can be calculated. Details of the methods followed in this study to obtain the apparent and physical activation volume can be found in [23]. The apparent activation volume (V_a) was obtained by fitting the following logarithmic equation to the first relaxation cycle of the series, if the relaxation indeed exhibits logarithmic variation of stress with time.

$$\Delta\sigma = -M\left(\frac{kT}{V_a}\right)\ln\left(1+\frac{t}{c}\right) \tag{3}$$

where V_a is the apparent activation volume, t is the time, $\Delta\sigma$ is the stress drop as a function of t, and c is the time constant. The physical activation volume (V) was calculated, using the following relationships

$$\Omega_r^{-1} = 1 - \left(\frac{MkT}{V_a}\sum_{1}^{n-1}\Delta\sigma_j\right)\ln\left[\frac{\left(\exp\left(\frac{-V_a\Delta\sigma_n}{MkT}\right)-1\right)}{\left(\exp\left(\frac{-V_a\Delta\sigma_1}{MkT}\right)-1\right)}\right] \tag{4}$$

$$V = \frac{V_a}{\Omega_r} \tag{5}$$

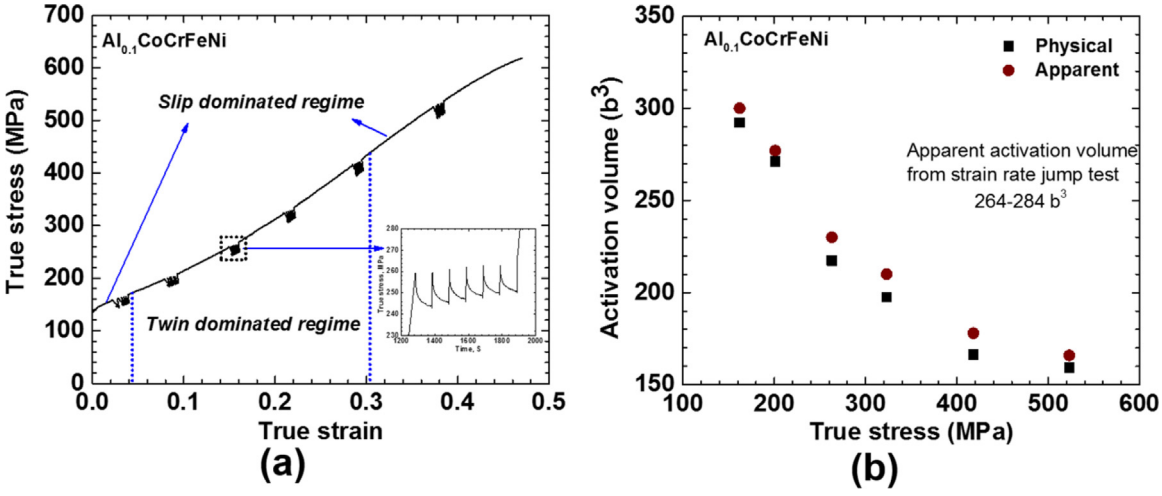

Fig. 5. (a) Repeated stress relaxation tests along the true stress–strain at various plastic strain and (b) variation in apparent and physical activation volume as a function of true stress.

The values of both the apparent and physical activation volume are plotted in Fig. 5(b). The apparent and the physical activation volumes were in the range of 300–166 b^3 and 292–159 b^3, respectively. One important point to be note is the closeness in the apparent activation volume obtained from two different types of tests, the strain-rate-jump and the relaxation tests. The physical activation volume obtained via the repeated stress relaxation tests is also surprisingly low. The interesting finding is that the physical activation volume of the CG HEA is significantly lower than the conventional CG FCC metals and alloys in annealed condition (usually on the order of thousands of b^3) [24]. This result clearly reveals the variation in the dislocation mobility in HEAs as compared to their conventional counterparts with same crystal structure.

4. Discussion

4.1. Peculiarity in the deformation mechanism and kinetics

A critical analysis for the observed large rate sensitivity of the flow stress and low activation volume in the coarse grained high entropy alloy will be carried out Section 4.1. So far, there are only two studies on the thermally activated deformation mechanisms of FCC HEA. In the as-cast CoCrFeNiMn HEA, Lee et al. [25] have observed a strain rate sensitivity and an apparent activation volume of 0.038 and 16 b^3, respectively. They hypothesized that the unique observation could be due to the relatively large Peierls barrier that was explained by Wu et al. [21]. In another study, Laktionova et al. [26] also observed a low activation volume of 122 b^3 at 300 K and the activation volume reduced with decreasing temperature. There was no explanation given on a possible mechanism for the abnormality. Hence, due to the peculiarity in the deformation mechanisms, it is important to consider all the possible mechanisms that could give rise to such results. In order to have an idealistic discussion on the effect of intrinsic microstructure on the observed dislocation mechanisms, both the m and V values immediately after the onset of the plastic flow will be considered. This will eliminate the complications arising from the increased forest dislocation density and its effect on *m* and *V*.

4.1.1. Comparison of m of HEAs with conventional alloys

Fig. 6 compares the strain rate sensitivity values obtained from the current study with the rate sensitivities of the CG, ultrafine-grained (UFG), and nanocrystalline conventional FCC materials. It is evident from the comparison that the rate sensitivity of the CG

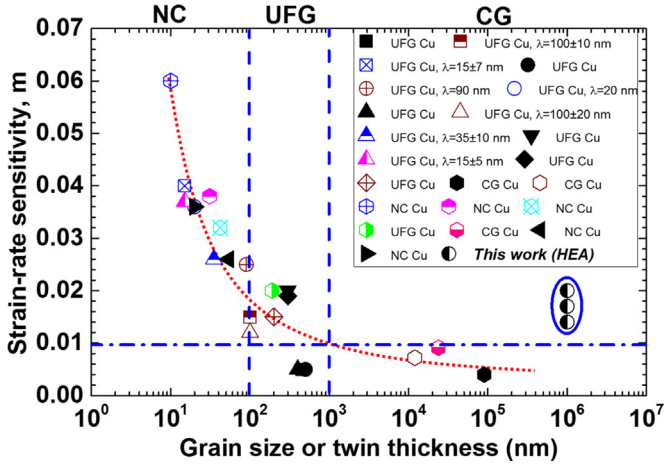

Fig. 6. Comparison of the strain rate sensitivity of the CG HEA with the strain rate sensitivities of the conventional CG, UFG, and NC FCC alloys [24,27–33].

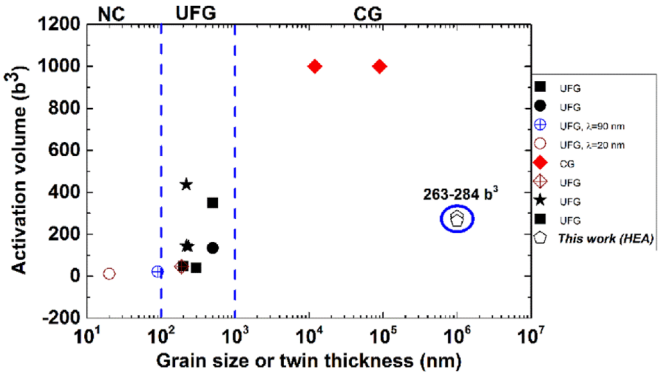

Fig. 7. Comparison of the activation volume of the CG HEA with the conventional CG, UFG, and NC FCC alloys [24,28,31,32,36].

HEA is higher than the conventional CG material and is equal to or higher than the UFG material. In the case of UFG conventional alloys, higher rate sensitivity is mainly attributed to the reduced mean free path of dislocations due to fine grain size, which is not the case for the present alloy. In another case, presence of nano twins in the UFG microstructure is also known to increase the rate sensitivity. The rate sensitivities of the materials with nano twins are same as the rate sensitivity of the CG HEA. Unlike the UFG microstructure with or without the nano twins, in the present case, there are no microstructural barriers (almost no grain boundaries or twin boundaries) that can impose a restriction on the dislocation movement to result in large rate sensitivity of the flow stress. The rate sensitivity of the flow stress is inversely proportional to the physical activation volume. Hence, as the activation volume of dislocations reduces, the strain rate sensitivity of the flow stress will increase. This concept still requires elaborate reasoning and discussion, which will be presented in the following Sections 4.1.2 and 4.1.3.

4.1.2. Comparison of V of HEA with conventional alloys

Fig. 7 compares the physical activation volume of the CG HEA with the literature data of CG and UFG FCC materials. As mentioned earlier, the activation volumes at small deformation strains will be considered for the discussion, which is in the range of 263–284 b^3. As can be clearly noted from Fig. 7, the activation volume of the CG HEA is at least 4–5 folds lower than what has been reported for the conventional CG FCC metals and alloys. The large activation volume in the conventional CG materials stems from the forest cutting mechanism of dislocations and always results in weak strain rate dependence of flow stress. When the grain size reduces to UFG regime, the activation volume of dislocations reduces drastically due to the presence of large fraction of GBs, which are now obstacles to the dislocation motion. Interestingly, the activation volume of the CG HEA is more or less equal to the UFG materials' activation volume. However, in the case of HEA, there are no submicron sized microstructural features that can obstruct the motion of dislocations. Given the unique nature of the activation volume, the reasoning should be elucidated based on solid fundamentals and the pertinent discussion is presented in the following.

In a study on the Cu single crystal, Bonneville et al. [34] observed an activation volume of 280 ± 65 b^3 at yield and attributed it to the cross-slip of dislocations. But, once the permanent deformation had started, a large activation volume close to 2600 b^3, a signature of forest cutting mechanism, was observed. Given the low SFE of HEAs, where the width of the stacking fault region is large, the dislocation cross-slip will be extremely difficult. Hence, based on the energetic considerations, abundant cross-slip and its consequence on the observed low activation volume are highly

unlikely. Another situation where low activation volume was reported in CG materials was in concentrated FCC binary solid solutions. Butt et al. [35] observed an activation volume of approximately 300 b^3 in Cu-20 at% Ni and Ni-20 at% Cu alloys. Furthermore, the activation volume continuously decreased with the increase in the solute content, which originated from the increased obstacle concentration to the dislocation motion. For the HEA composition of 97.6 at%(Co–Cr–Fe–Ni)-2.4 at%Al, the same range of activation volume was observed during the initial stages of the deformation, which will be subjected to further analysis in the Section 4.1.3.

4.1.3. Rationalizing the high value of m or low value of V in HEAs

4.1.3.1. Obstacle spacing. The physical activation volume of dislocations can be written as

$$V = b \times l^* \times \xi \tag{8}$$

where l^* is the length of the dislocation segment involved in the activation and ξ is the distance swept by the moving segment. As a result of the severe lattice distortion, b varies continuously with position, but for simplicity, b is considered as a constant. For a given b, in order to have low activation volume, both l^* and ξ should be small, which is the average area swept by the dislocation during the thermal activation. For the calculation of the distance between the thermal obstacles, sweep distance (ξ) of one Burgers' vector will be considered. Based on the above analysis, the physical activation volume of 284 b^3 will yield an average obstacle spacing of 72 nm. This is the highest possible value of obstacle spacing, because the sweep distance upon the thermal activation can only be increased from one to multiple Burgers vector, which will further reduce the obstacle spacing along the dislocation line. For example, l^* of 4.3 nm will be obtained when l^* and ξ are considered equal. Both the calculations hint on the large density of obstacles to the dislocation motion in HEAs.

4.1.3.2. Obstacle to dislocation motion in HEAs. So far, there is no clear understanding of how multiple elements impact the dislocation core and which of these elements could possibly be considered as obstacle to the dislocation motion. Therefore, understanding the origin of small activation volume in the light of concentrated solid solution becomes difficult. Wu et al. [21] considered an average contribution to yield strength arising from lattice friction and the presence of multiple elements rather than a separate contribution from solutes, which is a better treatment even in the current scenario. Besides, the presence and effect of solutes on dislocation motion can be clearly understood from the yield strength of the alloy. In order to exclude the strengthening contribution of solutes to the yield strength, all the other strengthening contributions should be accounted for. The grains in the present alloy were of mm in size, both XRD and TEM analyses show the absence of precipitates, and the as-received material was in well annealed condition. So, the contribution of grain size, dislocation density, and precipitation strengthening to the yield strength can be neglected. Therefore, the yield strength of the material is solely dependent on the Peierls–Nabarro stress and solid solution strengthening. Given the size of the Al atom as compared with other elements in the studied HEA, Al could very well act as a solid solution strengthener, which means it is an effective obstacle to the dislocation motion. However, since the atomic fraction of Al is very small in the studied HEA system, the solute obstacle density is extremely low. Hence the observed small activation volume is not solely controlled by the solute–dislocation interaction and necessitates further justification. For further discussion, the effect of Al as a solid solution strengthener will be considered as a part of the averaged lattice resistance to the dislocation movement.

4.1.3.3. Lattice distortion. In the absence of any possible microstructural elements that can obstruct the motion of the dislocation, the intrinsic nature of the HEA lattice itself will be considered as obstacles to the dislocation motion. As compared to conventional metals and alloys, the HEA lattice is heavily distorted, due to the atomic size variations of the constituent elements and the variations in binding energy between atom pairs. Wang [37] calculated the lattice distortion parameter, g, for various FCC and BCC HEAs. In the case of FeCoCrNi HEA, a g value of 0.0085 was obtained. Moreover the presence of Al, which is bigger than all the remaining four constituent elements, will increase the g value significantly. Chang et al. [38] have also observed the increase in the lattice strain energy as a function of number of elements added in the alloy. Guo et al. [39] experimentally observed a strong local structural distortion in a ZrNbHf BCC HEA. So in the present HEA system, the lattice distortion and the local variation in the lattice constant is certain. So far the effect of lattice distortion on lattice diffusion is somewhat understood, but the distortion effects on dislocation line energy and its motion needs to be explored.

4.1.3.4. Dislocation line energy and Peierls–Nabarro stress in HEAs. For further understanding, the atomic arrangements around dislocation line for a pure metal and for HEA lattice are given in Fig. 8 (a) and (c), and wherever applicable both the extremes will be compared. In the case of the pure metal, the atoms along the dislocation line are the same and also encounter the same environment, hence constant dislocation energy per length is expected. On the contrary, the environment is continuously varying along the dislocation line in HEAs, thus the energetics of the dislocation. Furthermore, as compared to the pure lattice, the HEA lattice is heavily distorted and possesses significant lattice strain energy. The introduction of dislocation in the already strained lattice will either decrease (by canceling out the opposite strain fields of the lattice and of the dislocation) or increase (by adding up the same strain fields) the local strain field. As a result, the dislocation line in HEAs will have varying strain fields, hence varying dislocation line energy, from very small to large values. The dislocation segment possessing the small and large strain will be in low and high energy states, respectively. The dislocation line energy, in general, is $E \sim \alpha G b^2$. The variation of shear modulus with alloying addition is known in the case of solid solutions and given the presence of multitude of elements in HEAs, the shear modulus will also vary continuously in the HEA lattice. The variation in the dislocation line energy will have effect on the dislocation motion as it progresses through the heavily distorted lattice with large intrinsic strain energy. In general, the intrinsic obstacle that the dislocation has to overcome during its movement is the lattice friction stress, also known as Peierls–Nabarro stress (P–N), τ_{PN}, and is given by [40]

$$\tau_{\mathrm{PN}} = \frac{2G}{1-\nu} \exp\left(\frac{-2\pi\omega}{b}\right) \tag{7}$$

where ν is the Poison's ratio, and ω is the dislocation width. As can be seen from the equation, the P–N stress is a strong function of ω and b. In the case of pure metal, both ω and b is constant for slip in close packed systems, hence the friction stress. On the contrary, since the HEA lattice is heavily distorted, there will be local variations in ω along the line. Thus, the fluctuations in ω and b will lead to variations in Peierls barrier height. Based on the aforementioned concepts, the dislocation energy as a function of displacement in pure metals and HEA lattice is aptly displayed as schematics in Fig. 8(b) and (d), respectively. The energetics trend shown in Fig. 8(d) can also be taken as the dislocation energy along the line. In the case of a pure metal, the atoms in the

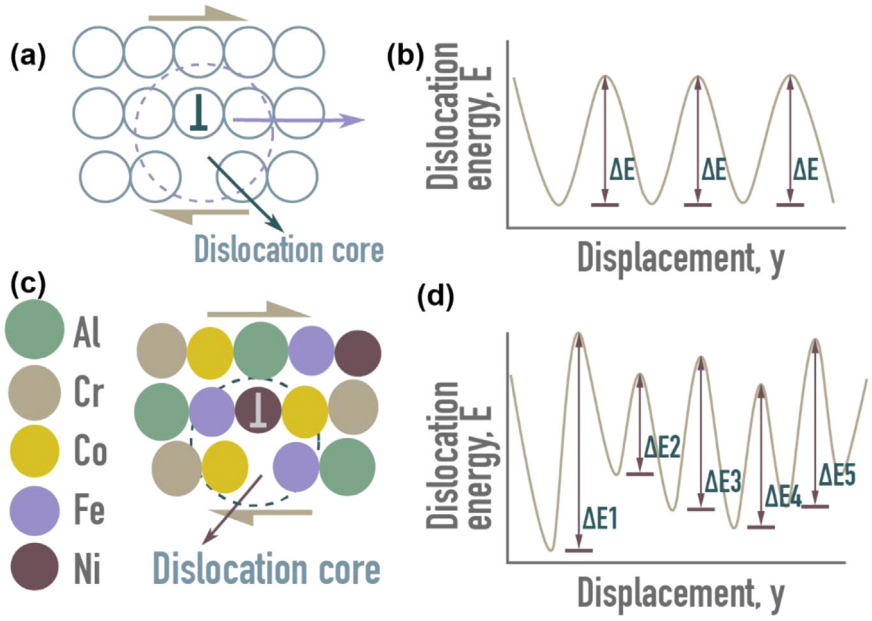

Fig. 8. Schematic of (a) atomic arrangement around dislocation core in pure metals and the corresponding dislocation energy with movement in (b), (c) atomic arrangement around dislocation core in HEA, and (d) the corresponding energy with displacement.

dislocation core encounter the same surrounding with displacement, thus the Peierls potential is periodic, like the periodicity of the crystal lattice, with a constant amplitude (ΔE), as shown in Fig. 8(c). On the contrary, in the case of HEAs, the dislocation line with the varying energy state has to move through the distorted lattice with the fluctuating energy states. This will result in the variation of the dislocation energy, i.e., varying amplitude (ΔE_1, ΔE_2, ΔE_3, and so on.), as it progresses in the slip system. For example, consider that a dislocation line has to move through the varying potential barrier. If a segment of the dislocation line is lying in a low energy state of the Peierls valley with the large Peierls energy barrier (small ω and large b), then the activation energy required to move that segment will be quite large. Unless the required activation energy is provided to overcome the energy barrier, that part of the dislocation segment becomes immobile, hence acting as a pinning point. Similar to the atomic traps discussed by Tsai et al. [8], in the current situation, the presence of the low energy dislocation states with large energy barrier will result in dislocation pinning points. The distribution of such pinning points in a 3-dimensional HEA lattice will affect both the length of the mobile dislocation segment and the length of the unobstructed dislocation sweep during strain rate jump tests. This hypothesis is a potential explanation for the observed low activation volume of dislocations in HEAs. To conclude, in the absence of all other possible obstacles, the only possible obstacle to the dislocation motion in HEAs is the intrinsic low energy valleys with the large fluctuation in lattice energies.

5. Conclusion

1. The strain rate sensitivity of the flow stress of the CG HEA was unusually large, as compared with the rate sensitivity of the conventional materials. The comparison of rate sensitivities at various grain sizes showed that the rate sensitivity of the FCC UFG material was closer to what was observed in this case.
2. Like strain-rate sensitivity, the physical activation volume of the dislocations also resulted in peculiar values. The activation volume of CG HEA was 4–5 folds lower than the activation volume of the conventional CG materials and equal to the activation volume of UFG materials.
3. The intrinsic HEA lattice distortion is likely to be responsible for the observed high rate sensitivity of the flow stress and low activation volume of dislocations.
4. Both the dislocation line energy and the Peierls potential energy in HEAs may have continuous variations, as opposed to the constant dislocation line energy and potential energy in the case of conventional metals and alloys. The presence of the varying potential energy barriers has been postulated to be the major obstacle hindering the dislocation line movement and the deep energy valleys in the distorted line energy profiles were the dislocation pinning points.
5. The average length of dislocation involved in thermal activation was calculated to be extremely low and aptly justifies the abundance of the intrinsic barriers in HEA to dislocation motion.

Acknowledgments

We would like to thank Center for Advanced Research and Technology (CART) for the microscopy facilities.

References

[1] J.W. Yeh, S.K. Chen, S.J. Lin, J.Y. Gan, T.S. Chin, T.T. Shun, Nanostructured high-entropy alloys with multiple principal elements: novel alloy design concepts and outcomes, Adv. Eng. Mater. 6 (2004) 299–303.
[2] B. Cantor, I.T.H. Chang, P. Knight, A.J.B. Vincent, Microstructural development in equiatomic multicomponent alloys, Mater. Sci. Eng. A 375–377 (2004) 213–218.
[3] Z. Tang, M.C. Gao, H. Diao, T. Yang, J. Liu, T. Zuo, Y. Zhang, Z. Lu, Y. Cheng, Y. Zhang, K.A. Dahmen, P.K. Liaw, T. Egami, Aluminum alloying effects on lattice types, microstructures, and mechanical behavior of high-entropy alloys systems, JOM 65 (2013) 1848–1858.
[4] J.Y. He, W.H. Liu, H. Wang, Y. Wu, X.Y. Liu, T.G. Nieh, Z.P. Lu, Effects of Al addition on structural evolution and tensile properties of the FeCoNiCrMn high-entropy alloy system, Acta Mater. 62 (2014) 105–113.
[5] Y. Zhang, T.T. Zuo, Z. Tang, M.C. Gao, K.A. Dahmen, P.K. Liaw, Z.P. Lu, Microstructures and properties of high-entropy alloys, Prog. Mater. Sci. 61 (2014) 1–93.
[6] Y.J. Zhou, Y. Zhang, Y.L. Wang, G.L. Chen, Solid solution alloys of AlCoCrFeNiTi$_x$ with excellent room-temperature mechanical properties, Appl. Phys. Lett. 90

(2013) 181904.
[7] J.W. Yeh, S.J. Lin, T.S. Chin, J.Y. Gan, S.K. Chen, T.T. Shun, C.H. Tsau, S.Y. Chou, Formation of simple crystal structures in Cu–Co–Ni–Cr–Al–Fe–Ti–V alloys with multiprincipal metallic elements, Metall. Mater. Trans. A 35 (2004) 2533–2536.
[8] C.H. Tsau, Phase transformation and mechanical behavior of TiFeCoNi alloy during annealing, Mater. Sci. Eng. A 501 (2009) 81–86.
[9] K.Y. Tsai, M.H. Tsai, J.W. Yeh, Sluggish diffusion in Co–Cr–Fe–Mn–Ni high-entropy alloys, Acta Mater. 61 (2013) 4887–4897.
[10] R.S. Mishra, N. Kumar, M. Komarasamy, Lattice strain framework for plastic deformation in complex concentrated alloys including high entropy alloys, Mater. Sci. Tech. 31 (2015) 1259–1263.
[11] N. Kumar, M. Komarasamy, R.S. Mishra, P.K. Liaw, 2015 (unpublished work).
[12] C.J. Tong, M.R. Chen, J.W. Yeh, S.J. Lin, S.K. Chen, T.T. Shun, S.Y. Chang, Mechanical performance of the $Al_xCoCrCuFeNi$ high-entropy alloy system with multiprincipal elements, Metall. Mater. Trans. A 36 (2005) 1263–1271.
[13] S. Fang, W. Chen, Z. Fu, Microstructure and mechanical properties of twinned $Al_{0.5}CrFeNiCo_{0.3}C_{0.2}$ high entropy alloy processed by mechanical alloying and spark plasma sintering, Mater. Des. 54 (2014) 973–979.
[14] K.B. Zhang, Z.Y. Fu, J.Y. Zhang, W.M. Wang, H. Wang, Y.C. Wang, Q.J. Zhang, J. Shi, Microstructure and mechanical properties of $CoCrFeNiTiAl_x$ high-entropy alloys, Mater. Sci. Eng. A 508 (2009) 214–219.
[15] Y.J. Zhou, Y. Zhang, Y.L. Wang, G.L. Chen, Microstructure and compressive properties of multicomponent $Al_x(TiVCrMnFeCoNiCu)_{100-x}$ high-entropy alloys, Mater. Sci. Eng. A 454–455 (2007) 260–265.
[16] Y.P. Wang, B.S. Li, M.X. Ren, C. Yang, H.Z. Fu, Microstructure and compressive properties of AlCrFeCoNi high entropy alloy, Mater. Sci. Eng. A 491 (2008) 154–158.
[17] F. Otto, A. Dlouhý, Ch Somsen, H. Bei, G. Eggeler, E.P. George, The influences of temperature and microstructure on the tensile properties of a CoCrFeMnNi high-entropy alloy, Acta Mater. 61 (2013) 5743–5755.
[18] M. Komarasamy, N. Kumar, Z. Tang, R.S. Mishra, P.K. Liaw, Effect of microstructure on the deformation mechanism of friction stir-processed $Al_{0.1}CoCrFeNi$ high entropy alloy, Mater. Res. Lett. 3 (2015) 30–34.
[19] B. Gludovatz, A. Hohenwarter, D. Catoor, E.H. Chang, E.P. George, R.O. Ritchie, A fracture-resistant high-entropy alloy for cryogenic applications, Science 345 (2014) 1153–1158.
[20] M.A. Hemphill, T. Yuan, G.Y. Wang, J.W. Yeh, C.W. Tsai, A. Chuang, P.K. Liaw, Fatigue behavior of $Al_{0.5}CoCrCuFeNi$ high entropy alloys, Acta Mater. 60 (2012) 5723–5734.
[21] Z. Wu, H. Bei, G.M. Pharr, E.P. George, Temperature dependence of the mechanical properties of equiatomic solid solution alloys with face-centered cubic crystal structures, Acta Mater. 81 (2014) 428–441.
[22] N. Kumar, M. Komarasamy, P. Nelaturu, Z. Tang, P.K. Liaw, R.S. Mishra, Friction stir processing of a high entropy alloy $Al_{0.1}CoCrFeNi$, JOM 67 (2015) 1007–1013.
[23] D. Caillard, J.L. Martin, Thermally activated mechanisms in crystal plasticity, Pergamon Mater. Ser. 8 (2003).
[24] J. Chen, L. Lu, K. Lu, Hardness and strain rate sensitivity of nanocrystalline Cu, Scr. Mater. 54 (2006) 1913–1918.
[25] D.H. Lee, I.C. Choi, M.Y. Seok, J. He, Z. Lu, J.Y. Suh, M. Kawasaki, T.G. Langdon, Nanomechanical behavior and structural stability of a nanocrystalline CoCrFeNiMn high- entropy alloy processed by high-pressure torsion, J. Mater. Res. 30 (2015) 2804–2815.
[26] M.A. Laktionova, E.D. Tabchnikova, Z. Tang, P.K. Liaw, Mechanical properties of the high-entropy alloy Ag0.5CoCrCuFeNi at temperatures of 4.2–300 K, Low Temp. Phys. 39 (2013) 630–632.
[27] Y.F. Shen, L. Lu, M. Dao, S. Suresh, Strain rate sensitivity of Cu with nanoscale twins, Scr. Mater. 55 (2006) 319–322.
[28] L. Lu, R. Schwaiger, Z.W. Shan, M. Dao, K. Lu, S. Suresh, Nano-sized twins induce high rate sensitivity of flow stress in pure copper, Acta Mater. 53 (2005) 2169–2179.
[29] M. Dao, L. Lu, Y.F. Shen, S. Suresh, Strength, strain-rate sensitivity and ductility of copper with nanoscale twins, Acta Mater. 54 (2006) 5421–5432.
[30] Y.M. Wang, E. Ma, Temperature and strain rate effects on the strength and ductility of nanostructured copper, Appl. Phys. Lett. 83 (2003) 3165–3167.
[31] Q. Wei, S. Cheng, K.T. Ramesh, E. Ma, Effect of nanocrystalline and ultrafine grain sizes on the strain rate sensitivity and activation volume: fcc versus bcc metals, Mater. Sci. Eng. A 381 (2004) 71–79.
[32] S. Cheng, E. Ma, Y.M. Wang, L.J. Kecskes, K.M. Youssef, C.C. Koch, U. P. Trociewitz, K. Han, Tensile properties of in situ consolidated nanocrystalline Cu, Acta Mater. 53 (2005) 1521–1533.
[33] L. Lu, S.X. Li, K. Lu, An abnormal strain rate effect on tensile behavior in nanocrystalline copper, Scr. Mater. 45 (2001) 1163–1169.
[34] J. Bonneville, B. Escaig, J.L. Martin, A study of cross-slip activation parameters in pure copper, Acta Met. 36 (1988) 1989–2002.
[35] M.Z. Butt, F. Aziz, D. Ali, Correlation between the temperature dependence of yield stress and the nature of solute distribution in Cu–Ni solid solutions, J. Alloy. Compd. 498 (2010) 102–106.
[36] R.W. Hayes, D. Witkin, F. Zhou, E.J. Lavernia, Deformation and activation volumes of cryomilled ultrafine-grained aluminum, Acta Mater. 52 (2004) 4259–4271.
[37] S. Wang, Atomic structure modeling of multi-principal-element alloys by the principle of maximum entropy, Entropy 15 (2013) 5536–5548.
[38] S.Y. Chang, C.E. Li, Y.C. Huang, H.F. Hsu, J.W. Yeh, S.J. Lin, Structural and thermodynamic factors of suppressed interdiffusion kinetics in multi-component high-entropy materials, Sci. Rep. 4 (2014) 1–8.
[39] W. Guo, W. Dmowski, J.Y. Noh, P. Rack, P.K. Liaw, T. Egami, Local atomic Structure of a high-entropy alloy: an X-Ray and neutron scattering study, Metall. Mater. Trans. 44A (2013) 1994–1997.
[40] D. Hull, D.J. Bacon, Introduction to Dislocations, Butterworth-Heinemann, UK, 2001.